than zirconium in $NiZr_2$ or to a higher foreign atom content in the $NiHf_2$ crystal examined.

Lattice dimensions of

$a_0 = 3{\cdot}220 \mp 0{\cdot}005$, $b_0 = 9{\cdot}820 \mp 0{\cdot}006$, $c_0 = 4{\cdot}12 \mp 0{\cdot}01$ Å

were determined from single crystal data for the phase NiHf. It is of interest to note that the dimensions a_0 and b_0 are somewhat smaller than those for the phase NiZr. However, the c_0 dimension is approximately the same for both phases. Since the atomic diameter of hafnium is slightly less than that of zirconium, it is probable that the c_0 dimension is controlled by the Ni–Ni contact.

Discussion

The packing efficiency in both the $C16$ and B_f structures is quite high with an average coordination number of 13 for NiZr and NiHf and of $13\frac{1}{3}$ for $NiZr_2$ and $NiHf_2$. The nickel atoms run through the $NiZr_2$ structure in straight linear chains with an interatomic spacing of 2·62 Å and with all chains parallel one to the other. A similar type of chain array is exhibited in $NiMg_2$ (Schubert & Anderko, 1951) wherein the Ni–Ni bond distance is 2·59 Å, but the linear chain arrangement differs from $NiZr_2$ in that the chains are parallel within a given layer but the orientation rotates 60° from one layer to the next.

A Ni–Ni bond distance of 2·62 Å is also found in NiZr where the closely bonded nickel atoms form wrinkled chains having a Ni–Ni–Ni bond angle of 103° 15′. In this latter case there is also a weaker interaction of each nickel atom with two additional nickels at 3·27 Å.

Only three out of eleven Zr–Zr bonds in $NiZr_2$ and none of the Zr–Zr bonds in NiZr are shorter than the 3·20 Å Zr–Zr bond in elemental zirconium. The Ni–Ni distances in the compounds are longer than the 2·48 Å Ni–Ni bond in elemental nickel. However, all of the Ni–Zr bonds are shorter than 2·84 Å which is the mean of the elemental bond distances. High packing efficiency plus an appreciable Ni–Zr interaction are thus presumed to be responsible for the stability of these compounds.

References

Bradley, A. J. (1935). *Proc. Phys. Soc.* **47**, 879.

Dauben, C. H. & Templeton, D. H. (1955). *Acta Cryst.* **8**, 841.

Fitzwater, D. R. (1958). Unpublished Ph.D. Thesis. Iowa State University, Ames, Iowa.

Fitzwater, D. R. & Williams, D. E. (1958). U.S. Atomic Energy Commission Report No. AL-140.

Friauf, J. B. (1927). *J. Amer. Chem. Soc.* **49**, 3107.

Hayes, E. T., Roberson, A. H. & Paasche, O. G. (1953). *Zirconium and Zirconium Alloys*, p. 275. Cleveland: Am. Soc. Metals.

Kiessling, R. (1949). *Acta Chem. Scand.* **3**, 595.

Kirkpatrick, M. E. (1958). Unpublished.

Libowitz, G. G., Hayes, H. F. & Gibb, T. R. P., Jr. (1958). *J. Phys. Chem.* **62**, 76.

Nelson, J. B. & Riley, D. P. (1945). *Proc. Phys. Soc.* **57**, 160.

Schubert, K. & Anderko, K. (1951). *Z. Metallk.* **42**, 321.

Thomas, L. H. & Umeda, K. (1957). *J. Chem. Phys.* **26**, 293.

Acta Cryst. (1962). **15**, 255

Structural Properties of $(Ba, Pb)_{1-\delta}(Ti, Nb)O_3$ Systems*

By S. Srikanta, V. B. Tare, A. P. B. Sinha and A. B. Biswas

National Chemical Laboratory, Poona-8, India

(*Received* 10 *January* 1961 *and in revised form* 19 *April* 1961)

The structural properties of several compositions in the quarternary system $PbTiO_3$–$BaTiO_3$–$BaNb_2O_6$–$PbNb_2O_6$, formed by high temperature solid state reaction of the constituent oxides, have been studied by the X-ray powder diffraction technique. Phases isomorphous with (i) cubic perovskite, (ii) tetragonal barium titanate, (iii) orthorhombic barium titanate, (iv) cubic pyrochlore, (v) orthorhombic lead niobate, (vi) tetragonal tungsten–bronze and (vii) orthorhombic barium niobate have been identified. The respective region of stability of each phase has been depicted on a two-dimensional phase-diagram.

Titanates and niobates of barium and lead are important ferroelectric materials and their structural and dielectric properties have been studied in detail (Känzig, 1957; Megaw, 1957). Some binary solid solutions of these compounds such as $BaTiO_3$–$PbTiO_3$ (Shirane & Suzuki, 1951; Shirane & Takeda, 1951), $PbTiO_3$–$PbNb_2O_6$ (Subba Rao, 1960), $BaTiO_3$–$BaNb_2O_6$ (Subba Rao & Shirane, 1959), and $PbNb_2O_6$–$BaNb_2O_6$ (Fran-

* N.C.L. Contribution No. 440.

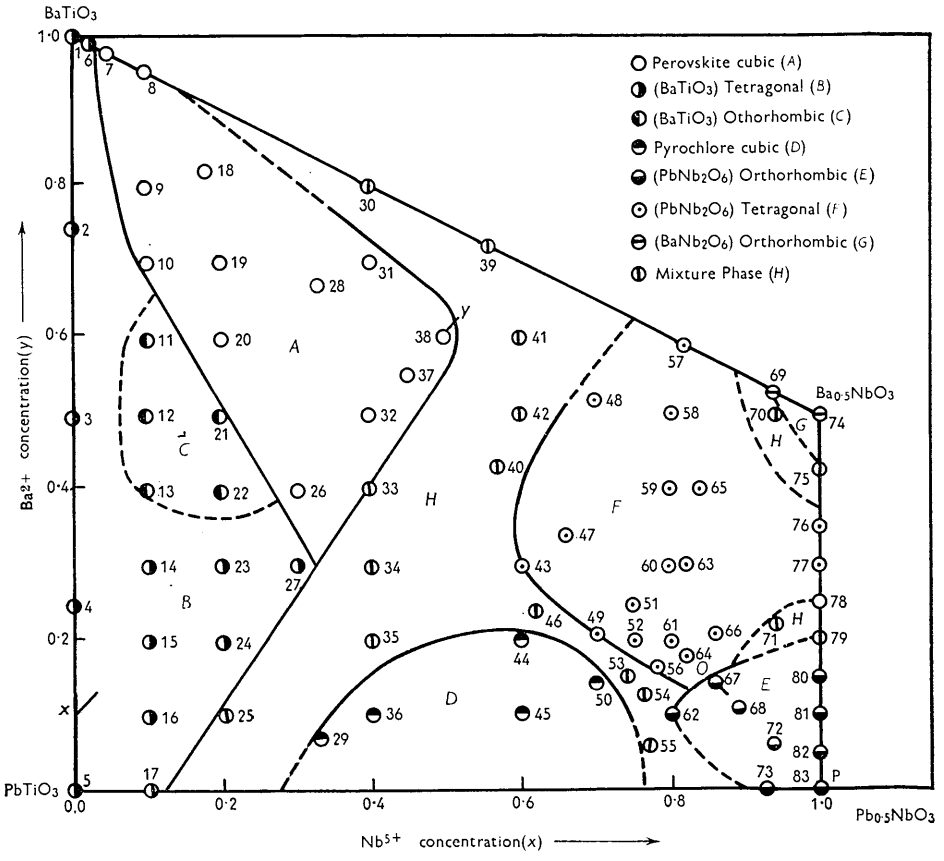

Fig. 1. Phase diagram

combe, 1960), have also been studied. However, the complete range of compositions possible for the $(Ba, Pb)_{1-\delta}(Ti, Nb)O_3$ system has not been covered. Therefore, several compositions in the quarternary system $PbTiO_3$–$BaTiO_3$–$BaNb_2O_6$–$PbNb_2O_6$ have been studied and the structural properties of these are described here.

The constituent compounds, $BaCO_3$(A.R.), TiO_2 (A.R.), PbO(A.R.) (previously heated to 700 °C. to convert any higher oxide to monoxide) and Nb_2O_5 (better than 99·9%) were weighed in the correct mole ratios, mixed in an agate mortar under alcohol, dried and heated to 1280–1300 °C. in PbO atmosphere for one hour and cooled in air. X-ray diffraction patterns of the products were taken on a 14 cm. Debye–Scherrer camera with Cu $K\alpha$ radiation filtered through a Ni foil. The d values were calculated (accuracy $\pm 0{\cdot}2\%$) and, since the phases present were isomorphous with known compounds, the reflections were indexed and then unit-cell parameters obtained. The density of a number of powder samples was determined using a density bottle. The reliability of these measurements was checked by determining the density of pure barium titanate samples. It was found that such measurements on powder samples always gave values lower than the theoretical, to a maximum extent of 5%. However, different measurements on the same samples agreed within $\pm 2\%$.

All the phases studied can be represented on a two-dimensional phase diagram shown in Fig. 1. A point (x, y) in the diagram represents the composition $Ba_yPb_{1-y-x/2}Ti_{1-x}Nb_xO_3$. The nominal compositions have been plotted and Pb loss during firing is assumed to be negligible. Seven types of phases are observed: (A) a cubic perovskite-type phase, (B) a phase isomorphous with tetragonal ferroelectric $BaTiO_3$, (C) a phase isomorphous with orthorhombic $BaTiO_3$, (D) a cubic pyrochlore-type phase, (E) a phase isomorphous with orthorhombic $PbNb_2O_6$, (F) a tetragonal tungsten-bronze-type phase and (G) a phase isomorphous with orthorhombic barium niobate. In addition to these there is a broad region (H) in which two or more phases coexist. The compositions studied have been indicated in the diagram. The phase boundaries are approximate because of the limited number of compositions studied.

(A) The cubic perovskite-type phase

The X-ray patterns of all compositions in the region A could be indexed on the basis of a cubic unit cell. There were no missing or extra reflections, but dif-

Table 1. *Density values for perovskite phases*

Structure	Phase no. (Fig. 1)	Composition: Formula unit	Measured density	Calculated no. of formula units per unit cell	Density calculated on the basis of $Z=1$
Cubic	9	$Ba_{0\cdot80}Pb_{0\cdot15}Ti_{0\cdot90}Nb_{0\cdot10}O_3$	5·81	0·90	6·44
	18	$Ba_{0\cdot82}Pb_{0\cdot09}Ti_{0\cdot82}Nb_{0\cdot18}O_3$	5·70	0·93	6·15
	20	$Ba_{0\cdot60}Pb_{0\cdot30}Ti_{0\cdot80}Nb_{0\cdot20}O_3$	6·30	0·96	6·57
	26	$Ba_{0\cdot40}Pb_{0\cdot45}Ti_{0\cdot70}Nb_{0\cdot30}O_3$	6·43	0·93	6·89
	28	$Ba_{0\cdot67}Pb_{0\cdot165}Ti_{0\cdot67}Nb_{0\cdot33}O_3$	5·83	0·94	6·20
	37	$Ba_{0\cdot55}Pb_{0\cdot225}Ti_{0\cdot55}Nb_{0\cdot45}O_3$	6·01	0·96	6·28
Tetragonal	23	$Ba_{0\cdot30}Pb_{0\cdot60}Ti_{0\cdot80}Nb_{0\cdot20}O_3$	7·04	0·97	7·25
	15	$Ba_{0\cdot20}Pb_{0\cdot75}Ti_{0\cdot90}Nb_{0\cdot10}O_3$	7·28	0·96	7·60
	16	$Ba_{0\cdot10}Pb_{0\cdot85}Ti_{0\cdot90}Nb_{0\cdot10}O_3$	7·40	0·96	7·73
Orthorhombic	12	$Ba_{0\cdot50}Pb_{0\cdot45}Ti_{0\cdot90}Nb_{0\cdot10}O_3$	6·60	0·96	6·86
	13	$Ba_{0\cdot40}Pb_{0\cdot55}Ti_{0\cdot90}Nb_{0\cdot10}O_3$	6·64	0·94	7·04
	22	$Ba_{0\cdot40}Pb_{0\cdot50}Ti_{0\cdot80}Nb_{0\cdot20}O_3$	6·30	0·91	6·89

fraction lines at high angles ($\theta > 55°$) were diffuse. The observed densities of some of the samples, given in Table 1, suggest that there is one formula unit of $A_{1-\delta}BO_3$ per unit cell. Thus for all compositions containing Nb^{5+}, the metal ion content is less than that required for an ABO_3 perovskite structure, leaving some of the metal sites vacant. Intensity calculations for a few diffraction lines were therefore carried out for two models: (i) with vacancies at A sites and (ii) with vacancies at B sites and corresponding Ti^{4+} or Nb^{5+} ions moving to A sites. The formula is $I \propto |F|^2.p.(1+\cos^2 2\theta)/(\sin^2\theta.\cos\theta)$ where $|F|$ is the structure amplitude and p is the multiplicity factor. Corrections for either the thermal vibrations or absorption were not applied. The agreement is better for the first model in which the vacancies are located at A sites.

(*B*) The tetragonal phase

This phase is isomorphous with the ferroelectric barium titanate and is stable for low concentrations of $Nb^{5+} < 0{\cdot}1$; with concentrations of $Nb^{5+} > 0{\cdot}1$, this phase is stable only if the Pb ion concentration is also high (Fig. 1). The X-ray photographs showed no extra reflections and the reflections for $\theta <$ about 55° were quite sharp but beyond this the lines were broadened progressively. The tetragonal distortion decreases as Pb^{2+} is replaced by Ba^{2+}, or as Ti^{4+} is replaced by Nb^{5+}. The variation of c/a with composition along the line XY of Fig. 1 is shown in Fig. 2. The density values for three phases in this region are given in Table 1 and they suggest that there is one formula unit per unit cell.

(*C*) The orthorhombic phase

A small island (C) is obtained on the diagram wherein the orthorhombic phase, isomorphous with the low-temperature $BaTiO_3$, is stable. The X-ray photographs for sample Nos. 12 and 21 were sharp, but those for Nos. 11, 13 and 22 were weak and diffuse. The phase

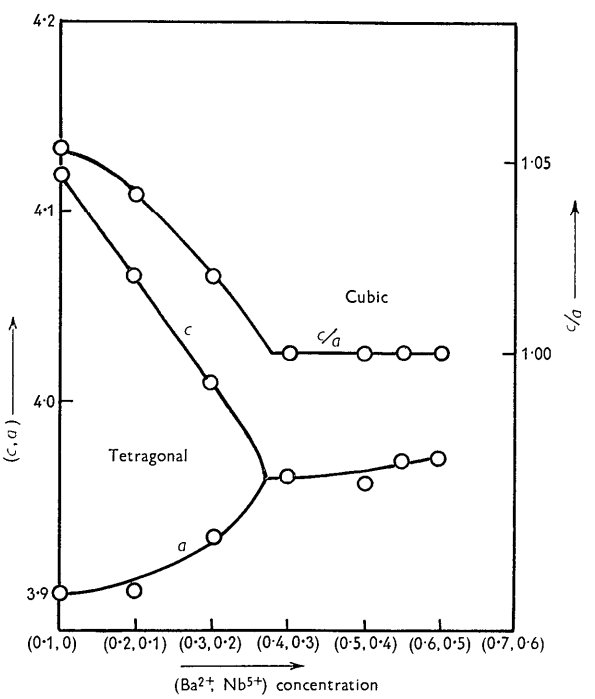

Fig. 2.

boundary in this region is therefore only approximately fixed. The measured density values (Table 1) suggest one formula unit per elementary cell.

(*D*) The cubic pyrochlore-type phase

The phases in the region (D) have a cubic pyrochlore type of structure (*Strukturbericht*, 1928–32). The small distortion found for $Pb_2Nb_2O_7$ (Cook & Jaffe, 1952; Jona, Shirane & Pepinsky, 1955) is absent in these compounds, suggesting that they may be paraelectric. The patterns were sharp up to the maximum observed θ (85°), but all the patterns had some very faint extra

Table 2. *Density values for pyrochlore phases*

Phase no. (Fig. 1)	Composition: Formula unit	Measured density	Calculated no. of formula units per unit cell	Number of ions per unit cell (Pb, Ba) 16*	(Nb, Ti) 16*	O 56*
36	$Ba_{0\cdot10}Pb_{0\cdot70}Ti_{0\cdot60}Nb_{0\cdot40}O_3$	6·35	15·8	12·6	15·8	47·4
44	$Ba_{0\cdot20}Pb_{0\cdot50}Ti_{0\cdot40}Nb_{0\cdot60}O_3$	6·19	16·7	11·7	16·7	50·1
45	$Ba_{0\cdot10}Pb_{0\cdot60}Ti_{0\cdot40}Nb_{0\cdot60}O_3$	6·15	16·2	11·3	16·2	48·6
29	$Ba_{0\cdot07}Pb_{0\cdot765}Ti_{0\cdot67}Nb_{0\cdot33}O_3$	6·43	15·7	11·5	15·7	47·1

* Number of ions present at these sites in ideal pyrochlore phase.

reflections; those from sample Nos. 29 and 36 could be attributed to the perovskite phase, and those from Nos. 44, 45 and 50 to the tetragonal tungsten–bronze-type of structure. However, it is estimated that the concentration of the extra phase is less than 2%. The compositions have the general formula $(Pb, Ba)_{1-\delta}(Nb, Ti)O_3$ where δ ranges from 0·15 to 0·375, concentrations of the Ba^{2+} ion from 0 to 0·225, and that of Nb^{5+} from 0·3 to 0·75. The densities of four samples in this region were measured and the number of $(Pb, Ba)_{1-\delta}(Nb, Ti)O_3$ molecules per unit cell was calculated (Table 2). It is found that there are vacancies at 16(*d*) sites and oxygen sites. The addition of oxygen during sintering accompanied by an increase in the valency of metal ions (possibly of Pb^{2+} ions) is considered unlikely from the following indirect arguments: (i) A partial change in valency would increase the electrical conductivity and hence the dielectric loss, which, however is not very high for these samples. (ii) If the same atom exists in more than one valence state in a compound, it is usually strongly coloured. However, these compounds have a light pink tint. (iii) $Pb_{0.75}NbO_{3.25}$ crystallizing in this structure is known to be deficient in oxygen (Cook & Jaffe, 1953).

(*E*) The orthorhombic phase

The phases in the region (*E*) crystallize with an orthorhombic structure isomorphous with lead niobate $PbNb_2O_6$. The X-ray patterns were sharp up to $\theta \simeq 40°$; but the higher-angle reflections were very weak. All the reflections observed for pure lead niobate, were present in the photographs and there were no extra reflections. A clear splitting was observed for the reflections 730, 820 and 840. It is found that the distortion (*b*/*a*) is maximum (1·014) for the pure lead niobate $PbNb_2O_6$ ($a = 17·65$, $b = 17·91$, $c = 7·736$ Å; $Z = 20$) and it decreases as Nb^{5+} and Pb^{2+} are replaced by Ti^{4+} and Ba^{2+} respectively along the line *PO* (Fig. 1). In the orthorhombic phase the oxygen octahedra are connected at the corners giving five and four-membered rings ('tunnel' and 'cage' sites respectively) at the centres of which are located the lead and barium ions (Francombe & Lewis, 1958). There are 24 such sites in a unit cell, 16 at the centres of five-membered and 8 at the centres of the four-membered rings. The pure $PbNb_2O_6$ has 20 Pb^{2+} ions per unit cell, which leaves 4 sites vacant. It is likely that the vacancies are at the cage sites, because this leaves the maximum number of Ba^{2+} and Pb^{2+} ions at the tunnel sites where they have a 15-fold coordination,

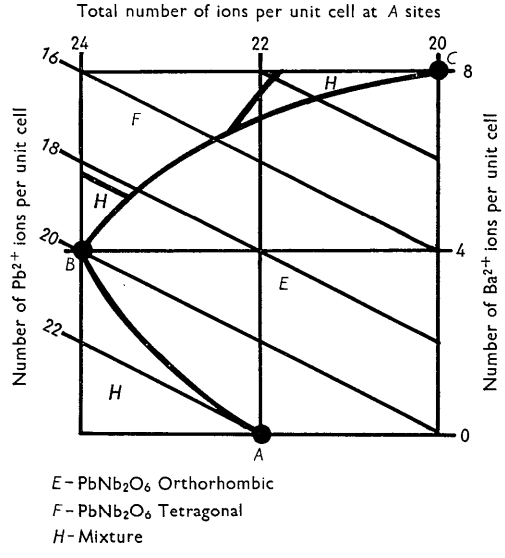

Fig. 3.

Table 3. *Density values for orthorhombic phases*

Phase no. (Fig. 1)	Composition: Formula unit	Measured density	Calculated no. of formula units per unit cell	Density calculated on the basis of $Z = 20$
62	$Ba_{0\cdot10}Pb_{0\cdot50}Ti_{0\cdot20}Nb_{0\cdot80}O_3$	6·33	18·7	6·77
68	$Ba_{0\cdot11}Pb_{0\cdot445}Ti_{0\cdot11}Nb_{0\cdot89}O_3$	6·39	19·4	6·58
72	$Ba_{0\cdot06}Pb_{0\cdot47}Ti_{0\cdot06}Nb_{0\cdot94}O_3$	6·46	19·5	6·63

Table 4. *Density values for tetragonal (tungsten–bronze) phases*

Phase no. (Fig. 1)	Composition: Formula unit	Measured density	Calculated no. of formula units per unit cell	No. of ions per unit cell		
				A(Ba, Pb)	*B*(Ti, Nb)	O
43	$Ba_{0\cdot30}Pb_{0\cdot40}Ti_{0\cdot40}Nb_{0\cdot60}O_3$	6·00	8·9	6·2	8·9	26·7
56	$Ba_{0\cdot166}Pb_{0\cdot444}Ti_{0\cdot22}Nb_{0\cdot78}O_3$	6·10	9·2	5·6	9·2	27·6
65	$Ba_{0\cdot40}Pb_{0\cdot18}Ti_{0\cdot16}Nb_{0\cdot84}O_3$	5·99	9·7	5·6	9·7	29·1
66	$Ba_{0\cdot21}Pb_{0\cdot36}Ti_{0\cdot14}Nb_{0\cdot86}O_3$	5·78	9·0	5·1	9·0	27·0

suggesting the energy is lower if the positive ions are surrounded by a larger number of negative ions. Also, the repulsive energy is lower if the ions are located in the larger holes, i.e. the tunnel sites.

The measured densities of some samples in this region are given in Table 2. It appears that in the orthorhombic structure the maximum number of *A* ions that can be accommodated at these sites depends on the Pb:Ba ratio in the compound. Thus, for the pure lead compound, the maximum value is 22 (point *A*, Fig. 3) which increases with increasing barium content (Fig. 3, *A* to *B*) till the maximum permissible value of 24 is attained. At still higher Ba:Pb ratio the maximum value of *A* again decreases from 24 to 20 along *BC* (Fig. 3). Possibly, large *A* ions tend to change the orthorhombic structure, to a tetragonal one.

(*F*) The tetragonal tungsten-bronze-type phase

The sample Nos. 57, 58, 65 and 76 gave weak and diffuse patterns, but all others in the region (*F*) gave patterns sharp up to $\theta=45°$ and comparable to the tetragonal tungsten–bronze structure. No extra reflections were observed.

The measured density values are given in Table 4. The number of ions at *A*, *B* and oxygen sites given in Table 4, have been calculated on the assumption that the ratio of metal to oxygen has remained unchanged during sintering. The compositions on the left side of the line at $x=0\cdot8$ are particularly interesting because if all the oxygen and the *B* sites were occupied, as in the tetragonal $PbNb_2O_6$ (Francombe & Lewis, 1958), the number of ions to be located at *A* sites would become greater than the number of available sites for such ions. However, the density values do not support this and suggest that the number of formula units per elementary cell is less than ten so that there are always some vacant *B* and oxygen sites.

(*G*) Barium niobate phase

Composition Nos. 69, 70 and 75 gave very weak diffraction patterns and the last two had some weak extra reflections not attributable to $BaNb_2O_6$ phase. It is, therefore, concluded that the pure $BaNb_2O_6$ structure ($a=12\cdot17$, $b=10\cdot25$, $c=3\cdot94$ Å; Francombe, 1960) is stable in a very narrow composition region. A rough phase boundary is shown in Fig. 1.

It is intended to publish the structural details and dielectric properties of these compounds later.

References

Cook, W. R. & Jaffe, H. (1952). *Phys. Rev.* **88**, 1426.

Cook, W. R. & Jaffe, H. (1953). *Phys. Rev.* **89**, 1297.

Francombe, M. H. (1960). *Acta Cryst.* **13**, 131.

Francombe, M. H. & Lewis, B. (1958). *Acta Cryst.* **11**, 696.

Jona, F., Shirane, G. & Pepinsky, R. (1955). *Phys. Rev.* **98**, 903.

Känzig, W. (1957). *Solid State Physics*, **4**, 5–180. New York: Academic Press Inc.

Megaw, H. D. (1957). *Ferroelectricity in Crystals*. London: Methuen.

Shirane, G. & Suzuki, K. (1951). *J. Phys. Soc., Japan*, **6**, 274.

Shirane, G. & Takeda, A. (1951). *J. Phys. Soc., Japan*, **6**, 329.

Strukturbericht (1928–32). *Z. Kristallogr.* **2**, 58.

Subba Rao, E. C. (1960). *J. Amer. Ceram. Soc.* **43**, 119, 439.

Subba Rao, E. C. & Shirane, G. (1959). *J. Amer. Ceram. Soc.* **42**, 279.